Title

Ubiquitous Low-Cost Functionalized Multi-Walled Carbon Nanotube Sensors for Distributed Methane Leak Detection

Journal

IEEE Sensors Journal, 16(24)

ISSN

1530-437X

Authors

Humayun, Tanim

Divan, Ralu

Stan, Liliana

et al.

Publication Date

2016

DOI

10.1109/jsen.2016.2581832

Ubiquitous Low-Cost Functionalized Multi-Walled Carbon Nanotube Sensors for Distributed Methane Leak Detection

Md Tanim Humayun, *Member, IEEE,* Ralu Divan, Liliana Stan, Daniel Rosenmann, David Gosztola, Lara Gundel, Paul A. Solomon, and Igor Paprotny, *Member, IEEE*

***Abstract*— This paper presents a highly sensitive, energy efficient, and low-cost distributed methane (CH_4) sensor system (DMSS) for continuous monitoring, detection, and localization of CH_4 leaks in natural gas infrastructure, such as transmission and distribution pipelines, wells, and production pads. The CH_4 sensing element, a key component of the DMSS, consists of a metal–oxide nanocrystal functionalized multi-walled carbon nanotube mesh, which, in comparison with the existing literature, shows stronger relative resistance change while interacting with lower parts per million concentration of CH_4. A Gaussian plume triangulation algorithm has been developed for the DMSS. Given a geometric model of the surrounding environment, the algorithm can precisely detect and localize a CH_4 leak as well as estimate its mass emission rate. A UV-based surface recovery technique making the sensor recover ten times faster than the reported ones is presented for the DMSS. A control algorithm based on the UV-accelerated recovery is developed, which facilitates faster leak detection.**

***Index Terms*— Methane, carbon nanotube, chemoresistor.**

I. Introduction

DESPITE having a shorter lifetime than CO_2, methane gas (CH_4) is more efficient in trapping radiation [1], [2]. The impact of CH_4 on climate change is projected to be 25 times stronger than that of CO_2 over a 100-year period [1], [3]. In 2013, 10% of emitted greenhouse gas in the USA was CH_4, while 29% of CH_4 emission was anthropogenic, i.e., the source is man-made, such as natural gas and petroleum systems [2]. Hence, the need exists for an extensive deployment of low cost, highly sensitive, selective and continuous CH_4 monitoring networks throughout the natural gas extraction and distribution infrastructure.

In this paper, we describe a low-cost microfabricated CH_4 sensing system and a corresponding detection algorithm for pinpointing leaks in natural gas infrastructures. Our novel Gaussian plume triangulation algorithm can precisely detect and localize a CH_4 leak and estimates its mass emission rate (MER), if a geometric model of the surrounding environment is provided. This algorithm complements our novel metal oxide nanocrystals (MONC) functionalized MWCNT mesh based micro-fabricated CH_4 sensing element, which is the key constituent for the distributed CH_4 sensor system (DMSS) described in this work. A control algorithm for the plume mapping process based on UV-accelerated surface recovery of the functionalized MWCNT CH_4 sensor is also described. The reminder of this paper is structured as follows: Section II presents a review on existing methane monitoring technologies; the fabrication process and characterization of the MONC functionalized MWCNT methane sensor are presented in Section III; Section IV explains the triangulation algorithm for remote methane leak detection; a UV-recovery-based plume mapping algorithm is described in Section V; Section VI describes sensor response time and possible interference during outdoor application of the sensor; Section VII summarizes the paper. A preliminary version of this work was previously presented [4].

II. Related Work

Three types of CH_4 sensors have been generally reported in literature: (a) sensors based on filtered infrared (IR) absorption [5], [6], (b) sensors based on Cavity Ring-Down Spectroscopy (CRDS) [3], [7], (c) metal-oxide based chemoresistor/chem-FET [8]–[10].

Filtered IR sensors, which detect CH_4 in the ppm range from its absorption of IR light, have been widely used in gas gathering, transmission and distribution pipelines. A number of other hydrocarbon gases also have absorption bands/lines in the same spectral region as CH_4, hence, IR detectors are not methane-specific [5]. Also, they are expensive and often need to be cooled to achieve better signal-to-noise ratios, increasing their power consumption [6].

Sensors based on cavity ring-down spectroscopy (CRDS) utilize an optical detection scheme to conduct fast mobile

Manuscript received March 2, 2016; revised May 19, 2016; accepted June 1, 2016. Date of publication June 16, 2016; date of current version November 17, 2016. This work was supported in part by the Center for Nanoscale Materials, Argonne National Laboratory, an Office of Science user facility, was supported by the U. S. Department of Energy, Office of Science, Office of Basic Energy Sciences, under Contract DE-AC02-06CH11357. The project is in part funded by the College of Engineering, University of Illinois, Chicago, IL, and by a Grant from Aclima Inc., under Award 2015-07496. The associate editor coordinating the review of this paper and approving it for publication was Prof. Hongrui Jiang.

M. T. Humayun and I. Paprotny are with the Department of Electrical and Computer Engineering, University of Illinois at Chicago, Chicago, IL 60607 USA (e-mail: mhumay2@uic.edu; paprotny@uic.edu).

R. Divan, L. Stan, D. Rosenmann, and D. Gosztola are with the Center for Nanoscale Materials, Argonne National Laboratory, Lemont, IL 60439 USA (e-mail: divan@anl.gov; lstan@anl.gov; rosenmann@anl.gov; gosztola@anl.gov).

L. Gundel is with the Lawrence Berkeley National Laboratory, Berkeley, CA 94720 USA (e-mail: lagundel@lbl.gov).

P. A. Solomon is with the U.S. Environmental Protection Agency, Las Vegas, NV 89119 USA (e-mail: solomon.paul@epa.gov).

Digital Object Identifier 10.1109/JSEN.2016.2581832

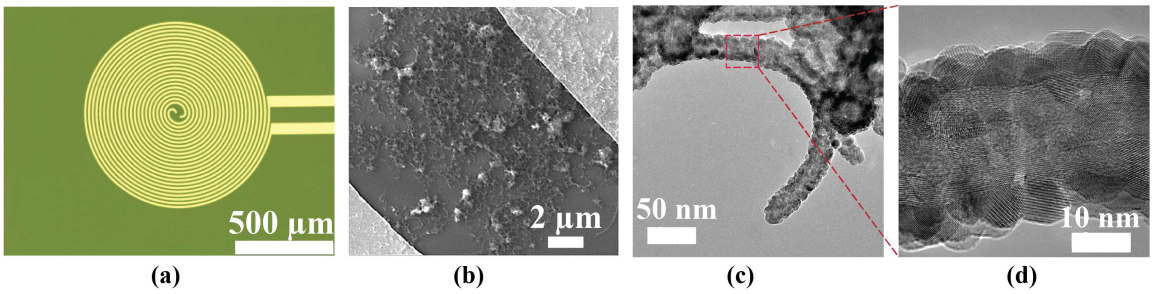

Fig. 1. (a) Optical microscope image of a functionalized MWCNT based CH_4 chemoresistor sensor. (b) Scanning electron microscope image of the sensor illustrating metal oxide nanocrystals functionalized MWCNT deposited between two metal electrodes. (c) Transmission electron microscope (TEM) image of a ZnO nanocrystals functionalized MWCNT. (d) High resolution TEM image showing lattice fringes of ZnO nanocrystals on the surface of a MWCNT.

leak measurements. The isotopic ratios of the stable isotopes of both carbon and hydrogen, along with the atmospheric concentration and distribution of the CH_4, can be used to derive the location and magnitude of CH_4 sources. However, the principal limitation of CRDS is its complex structure and immobility making the detection technology significantly expensive [3], [7].

Metal-oxide chemo-resistor or chem-FET are widely used to detect methane [8]–[10]. Continuous heating is necessary to initiate the surface chemisorption process of oxygen on these metal-oxides. Consequently, the power consumption by these sensors is high (hundreds of mWs and higher) [8]–[10].

CNT based gas sensors have the following properties which are uniquely attributed to their nano-scale dimension: (1) great adsorptive power due to large surface area to volume ratio, (2) stronger modulation of electrical properties (i.e., resistance) upon exposure to target gases, (3) tunable electrical properties correlated with composition and size, and (4) compatibility with low-power micro and nano-electronics [11], [12].

Thus, ppm level of gas detection has been reported using CNT based chemoresistive sensors with a power consumption of only few mWs [13]–[15].

III. Sensor Fabrication and Testing

We fabricated MONC functionalized MWCNT CH_4 chemoresistor sensors which are able to detect 10 ppm of CH_4 in dry air at room temperature. A lift-off based photolithography process was implemented to fabricate a set of interdigitated metal (Au/Cr) electrodes on top of SiO_2/Si substrates (Fig. 1a). The gap between the electrodes varied in the range of 5 μm to 10 μm. A solution of MWCNTs/ethanol was drop deposited on the interdigitated electrodes following a baking at 75 °C temperature to remove the solvent. MWCNTs network created a conductive bridge between the two pairs of electrodes (Fig. 1b). The MWCNTs were subsequently surface-activated by O_2 plasma and UV-O_3 for duration of 5 mins to 1 hr. The surface activated MWCNTs network was functionalized with metal oxides such as ZnO [16] or SnO_2 [17] nanocrystals using atomic layer deposition (ALD). Fig. 1c is a transmission electron microscope (TEM) image of a ZnO functionalized MWCNT sample showing uniform distribution of the "spherical" ZnO nanocrystals on the MWCNT surface. Clearly visible lattice fringes of ZnO in the high resolution TEM image suggest high crystal quality of ZnO nanocrystals (Fig. 1d).

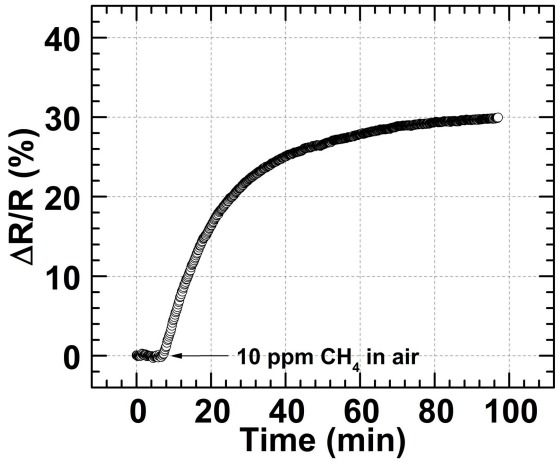

Fig. 2. Relative resistance change of the ZnO-MWCNT sensor as a function of time while the sensor was exposed to a mixture of 10 ppm of CH_4 in dry air at room temperature. The RH inside the test chamber was kept constant during the test.

The fabricated sensors were tested at room temperature inside an enclosed chamber where 10 ppm CH_4 in dry air mixture was introduced while maintaining a constant (approximately 5 %) relative humidity (RH). The relative resistance change of the sensor ($\Delta R/R = (R_{CH_4} - R_{air})/R_{air}$) were recorded as a function of time and was found to increase in a monotonic fashion in presence of the CH_4 mixture (Fig. 2).

IV. Triangulation Algorithm for Remote Leak Detection

In this work, we present a novel Gaussian plume triangulation algorithm which, given a geometric model of the surrounding environment, can precisely detect and localize a CH_4 leak while estimating its mass emission rate. Note that we assumed a faster response sensor comparing to our fabricated MONC-MWCNT sensors. Our current fabrication is focused on reducing the response time of the MONC-MWCNT sensors.

In the proposed approach the MWCNT sensors will be mounted on nodes distributed close to a production pad or pipeline. Fig. 3 illustrates a system where the sensor nodes are distributed on a 10 m X 10 m grid on an area around a natural gas production well head. The approach

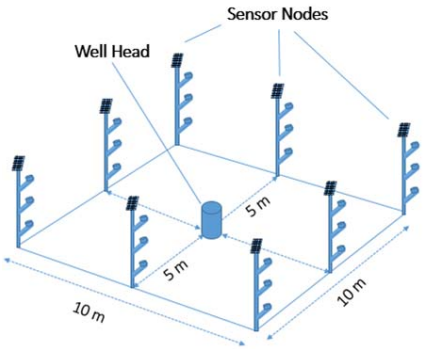

Fig. 3. The system diagram of distributed methane sensors on a 10 m × 10 m model production pad.

relies on varying wind direction to sweep a plume of CH_4 emanating from a nearby leak (e.g. from the well head) across two or more sensors. Once the plume moves across a sensor location due to variations in wind direction, a plume distribution can be reconstructed by using the triangulation detection algorithm which is based on Gaussian plume model.

However, the DMSS can be extended to an arbitrary spatial sensor distribution. The approach relies on varying wind direction to sweep a plume of CH_4 emanating from a nearby leak across two or more sensors. Using the National Wind Technology Center dataset [18] as a baseline (obtained near Boulder, Colorado, US) wind rose plots were analyzed for 4 randomly chosen 18 days period in 2013. The average (prevailing) direction of wind was West or South-West with the wind covering more than 180° in the course of 18 days. This is assumed to be representative wind distribution and is later used by the leak detection algorithm.

A. Gaussian Plume Model

A Gaussian plume model [19] is devised for estimating the evolution of a plume emanating from a ground level leak for different wind directions and speeds. For a constant leak rate and a constant wind speed the ground level concentration χ (μg/m^3) at the point (x,y) may be written using the Gaussian plume equation as:

$$\chi(x, y, z_0, H) = \frac{Q \times 10^6}{\pi \sigma_y \sigma_z U} exp[-\frac{1}{2}(\frac{y}{\sigma_y})^2] \times exp[-\frac{1}{2}(\frac{H}{\sigma_z})^2] \quad (1)$$

where Q (μg/s) is the source emission rate, U(m/s) is the wind speed at stack height, σ_y and σ_z are the standard deviation of concentration distributions in crosswind and vertical directions respectively, H (m) is the effective stack height (the sum of stack height and plume rise), x (m) is the downwind distance from the stack, y (m) is the crosswind distance from the plume centerline, and z_0 (m) is the vertical distance from ground level, assumed to be zero.

From the fitting of Pasquill-Gifford-Turner diffusion coefficient curves, σ_y and σ_z are given as:

$$\sigma_y = cx^d \quad (2)$$

$$\sigma_z = ax^b \quad (3)$$

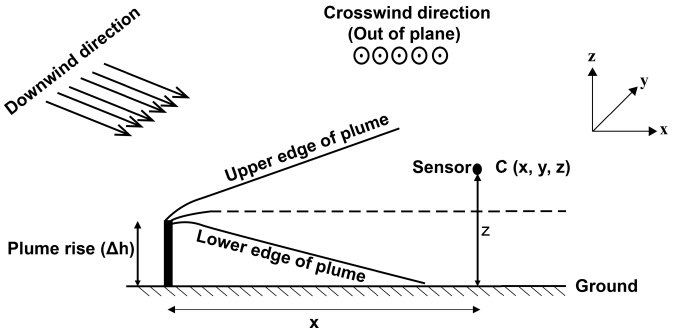

Fig. 4. Illustration of the Gaussian plume dispersion model.

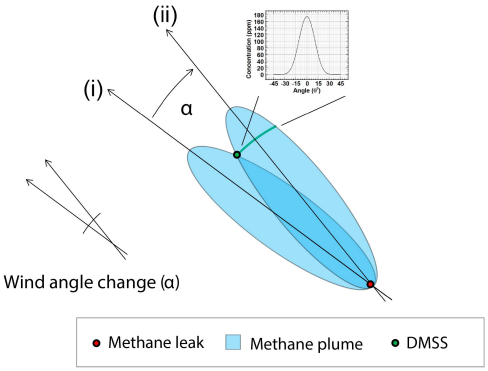

Fig. 5. CH_4 plume propagating across a sensor node due to varying wind direction. This example assumes that wind velocity is constant as the angle varies.

where, constants a, b, c, and d are 0.112, 0.91, 0.197, and 0.908, respectively. Fig. 4 illustrates the Gaussian plume dispersion model. Note that although the Gaussian plume model might not be applicable (due to turbulence) during high (> 6 m/s) wind velocities, such wind speeds are considered uncommon, and sensor readings during those times will be ignored without significantly compromising the desired 18 day detection time. Similarly, the readings at wind speeds below 1 m/s will be omitted.

If valid, the Gaussian plume distribution at a point x downstream of the leak is uniquely defined by the dispersion parameters, which are assumed constant, the wind velocity U (m/s) and the emission rate at the leak Q.

B. Single Plume Leak Estimation

Once a plume moves across a sensor location due to variations in wind direction, a plume distribution can be reconstructed. This concept is illustrated on Fig. 5. As CH_4 plume from a nearby leak rotates from position (i) to position (ii), the sensor signal records the plume profile. The below analysis assumes the wind velocity is constant, which may not be the case; however, the theory extends easily to cases with variable wind velocity.

Calculated distributions of a CH_4 plume using Eq. (1) are plotted on Fig. 6 as a function of rotating wind direction for two different wind velocities (1 ms^{-1} and 5 ms^{-1}). The distribution of methane concentration was calculated at different points along the centerline of the plume (2 m – 14 m distances from the leak location). The mass emission rate

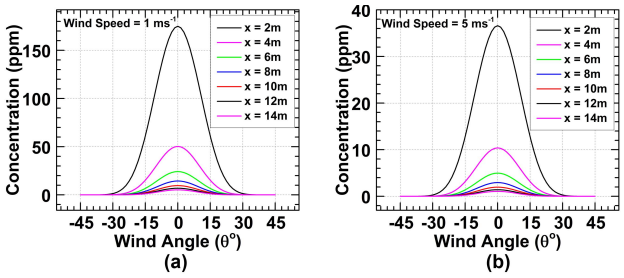

Fig. 6. Distribution of CH_4 plume as a function of wind angle for two different wind speeds: (a) 1 m/s and (b) 5 m/s. The distribution of methane concentration was calculated at different points along the centerline of the plume (2 m – 14 m distances from the leak location). "Wind angle" is defined as the angle between the wind direction and the straight line connecting the location of the leak and the sensor. It also represents the rotation of the wind direction. The mass emission rate was assumed to be 0.032 g/s or 6 standard cubic feet per hour (SCFH).

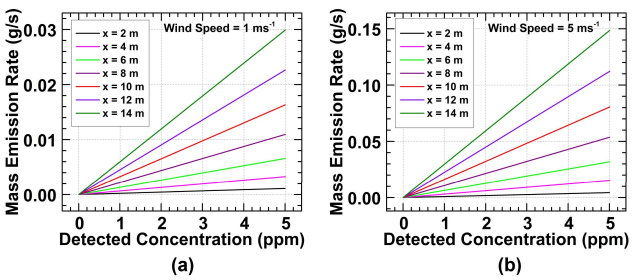

Fig. 7. Mass emission rate (g/s) as a function of maximum detected CH_4 concentration (ppm) by a sensor located at different distances from the leak location (2 m – 14 m) along the centerline of the plume. The wind speed was assumed as 1 m/s in (a), and 5 m/s in (b), respectively.

was assumed to be 0.032 g/s or 6 standard cubic feet per hour (SCFH).

The down-wind coordinate (x) from the leak (the distance to the sensor from the leak along the centerline of the plume), can be extrapolated from the peak concentration λ (ppm) and wind velocity U (m/s) by numerically solving the following equation:

$$log(ca) + (b+d)logx = log\frac{QV_m \times 10^3}{M\lambda\pi U} - \frac{(\Delta h)^2}{2a^2x^{2b}} \quad (4)$$

where, λ is the concentration of the detected CH_4 in parts per millions (ppm), M is the Molar mass of CH_4 (g/mol), V_m is the molar volume of an ideal gas at standard temperature and pressure. The plume rise due to the buoyancy of CH_4 (Δh) is calculated as

$$\Delta h = \frac{Ex^{\beta}}{\overline{u^{\alpha}}} \quad (5)$$

where, for a stable atmosphere, $\alpha = 1$, $\beta = 2/3$, and $E = 1.6F^{(1/3)}$, where F is the buoyancy flux parameter, defined as

$$F = \frac{gd^2V_s(T_s - T_a)}{4T_s} \quad (6)$$

where g is acceleration due to gravity (9.8 ms^{-2}), d (m) is stack diameter, V_s (m/s) is stack exit velocity, T_a (°C) is ambient temperature at stack height, and T_s (°C) is stack exit temperature at stack height.

Once distance to the leak (x) is established, the following formula can be used to calculate the leakage rate:

$$Q = \frac{\lambda M}{V_m} \times \frac{\pi\sigma_y\sigma_z U}{10^6} \times exp[\frac{1}{2}(y/\sigma_y)^2] \times exp[\frac{1}{2}(H/\sigma_z)]^2 \quad (7)$$

where Q (g/s) is the mass emission rate (MER) of the leak. Consequently, estimation of the MER of a single leak is possible by scanning the leak distribution plume.

The mass emission rate (MER) of the leak (g/s) as a function of maximum detected CH_4 concentration by sensors located at various distances along the plume centerline is illustrated in Fig. 7.

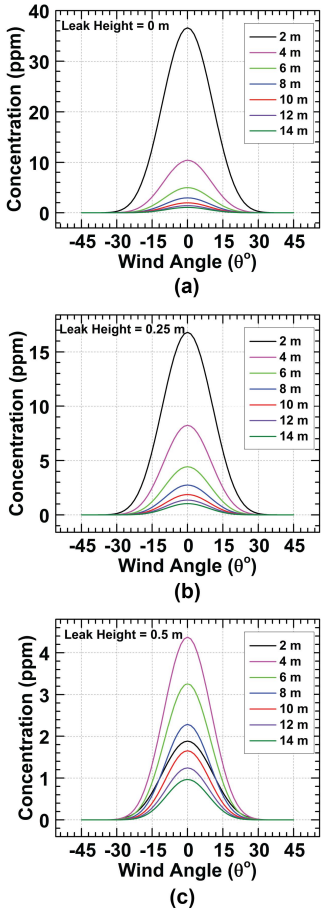

Fig. 8. Distribution of CH_4 plume as a function of wind angle for three different leak heights: (a) 0 m, (b) 0.25 m and (c) 0.5 m. The distribution of methane concentration was calculated at different points along the centerline of the plume (2 m – 14 m distances from the leak location). The wind speed is assumed to be 5 m/s. The mass emission rate was assumed to be 0.032 g/s or 6 standard cubic feet per hour (SCFH).

The methane plume distribution at the sensor location is dependent on the vertical position of the leak, i.e., leak height. The distributions of a CH_4 plume as a function of wind angle for three different leak heights (0 m, 0.25 m, and 0.5 m) are plotted in Fig. 8. The sensor experiences strongest plume concentration for ground level leak (Fig. 8a). As the leak height increases, the plume concentration experienced by the sensor becomes weaker (Fig. 8b and c). The plume rise due to the buoyancy of CH_4 (Δh) is included in the plume distribution calculation. The distribution of methane concentration

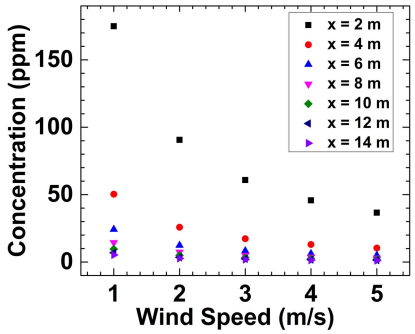

Fig. 9. The peak concentration of a CH_4 plume at its centerline as a function of wind speed (1 m/s – 5 m/s).

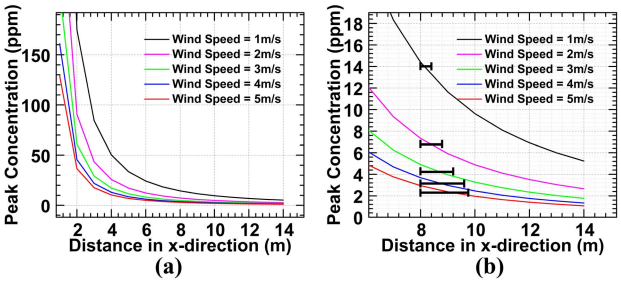

Fig. 10. (a) Peak concentration of the plumes at various wind speeds (1ms^{-1} – 5 ms^{-1}) for different distances along the plume centerline (a) 2 m – 14 m, and (b) 7 m – 14 m. The error bars correspond to uncertainty in sensor distance due to LDL quantization, assuming an effective LDL of 1 ppm.

was calculated at different locations of the sensor along the centerline of the plume (2 m – 14 m distances from the leak position). The wind speed is assumed to be 5 m/s. The mass emission rate was assumed to be 0.032 g/s or 6 SCFH.

The peak concentration of a CH_4 plume at its centerline as a function of wind speed (1 m/s –5 m/s) is plotted in Fig. 9. These results are based on a simulation that assumes the leak is at ground level and that the mass emission rate from the leak was assumed to be 0.032 g/s or 6 SCFH and held constant. The distribution of methane concentration was calculated at different distances from the methane leak (2 m–14 m away from the leak). The plume rise due to the buoyancy of CH_4 (Δh) is included in the plume distribution calculation. The response of the sensor is larger at slower wind velocities. As the wind velocity increases the sensor response becomes smaller following a simple logarithmic decay (Fig. 9). Our calculation also suggests that considering an LDL of 2 ppm, the sensor will be able to detect CH_4 leaks in the range of 0.09 m/s to 9 m/s of wind speed provided that the sensor is located at 2 m distance on the centerline of the plume.

C. Quantifying Sensor Response and Noise

The shape of the plume recorded by the sensor depends on its lower detection limit (LDL). Single ppm CH_4 sensitivity is currently achieved using our MONC-MWCNT chemoresistor sensor [16], [17]. Consequently, we defined the LDL of the sensors as 1 ppm. Our ongoing research is focused on achieving sub-ppm detection limit. For this particular analysis, we estimated the integration time of the sensor as one minute. Assuming an error of $\pm LDL$, the error in plume height and plume width can be estimated. Errors in other factors, such as wind speed or wind direction will also contribute to the error of the sensor, but can be reduced by increasing integration time.

Fig. 10 shows the center point plume concentration as a function of wind speed ($1 - 5 \text{ ms}^{-1}$) and distance, for a point leak with mass emission rate of 6 SCFH. The error bars (Fig. 10) indicate the distance uncertainty at 8 m distance from the leak (Note 14 m is the largest distance from the leak in a 10 m × 10 m grid).

The wind data (National Wind Technology Center dataset obtained near Boulder, Colorado, US [18]) suggests that errors contributed by wind velocity and wind direction can be reduced by improving the data integration time of the sensor. To obtain better understanding on the errors related to wind speed/direction and the integration time of the sensor, future work should involve further simulations based on real-time measured wind velocity and wind direction, i.e., to model variation in wind direction and velocity in different time segments and error estimation based on sensors response time.

V. UV-Recovery-Based Plume Mapping Algorithm

Once a chemoresistor CH_4 sensor is exposed to CH_4, the response back to baseline resistance, i.e. recovery, is slow [13], [16]. We have developed a UV recovery technique for the ZnO-MWCNT CH_4 sensor that improves the recovery time (about 3 min) by a factor of 10 compared to published studies (about 30 min) [13] as well as our previous work [16]. Optoelectronic application of the ZnO-CNT, such as optical switching has been reported before [20], [21]. ZnO is a wide-bandgap semiconductor (3.37 eV) with a large exciton binding energy (60 meV) [21], which facilitates photo-induced enhancement of sensor recovery. UV irradiation lowers the energy barrier of desorption of CH_4 molecules from the functionalized CNT surface [13], which increases the removal of CH_4 from the CNT surface and shortens the recovery time of the sensor [13]. Once the electron-hole pairs are generated in the functionalizing ZnO nanoparticles as a result of UV exposure, electrons migrate to the surface and help to desorb the CH_4 molecules [22].

Results presented in this section show that there is an improvement in the recovery time resulting from the UV exposure of the MONC-MWCNT sensor. To study the UV recovery, the sensor was first exposed to 10 ppm CH_4 in air for 30 min. Without interrupting the flow of CH_4, the sensor was irradiated with a UV light (390 nm) until the sensor returned to its baseline resistance (Fig. 11). A recovery time of about 3 minutes was observed, which is a 10 times improvement compared to past results even when the CH_4 flow was interrupted [13], [16].

Consequently, a UV-recovery-based mapping algorithm has been proposed for the ZnO-MWCNT sensor. The flowchart of the UV-recovery plume mapping algorithm is shown in Fig. 12. The complete mapping mechanism is decomposed into three phases. In the first phase, the sensor is initiated to sense the plume (phase 1: initiate search for plume). In phase 2, when a plume hits the sensor, it starts to respond. The value will be set little higher than the maximum resistance to avoid false detection of the plume. A resistance increment of 11%

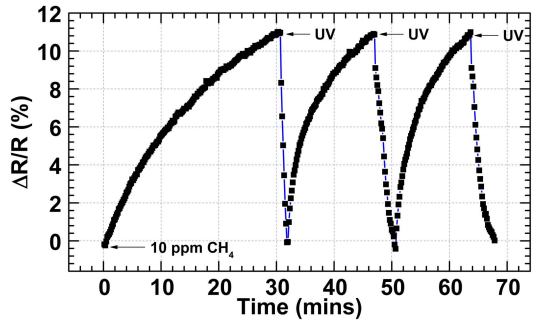

Fig. 11. Relative resistance ($\Delta R/R = (R_{CH_4} - R_{air})/R_{air}$) of the ZnO-MWCNT sensor while exposed to 10 ppm CH_4 in air and recovered by irradiating with a 390 nm wavelength UV light (without stopping the CH_4 flow). Average recovery time was about 3 min. After each UV exposure, the sensor peaked in about 15 min.

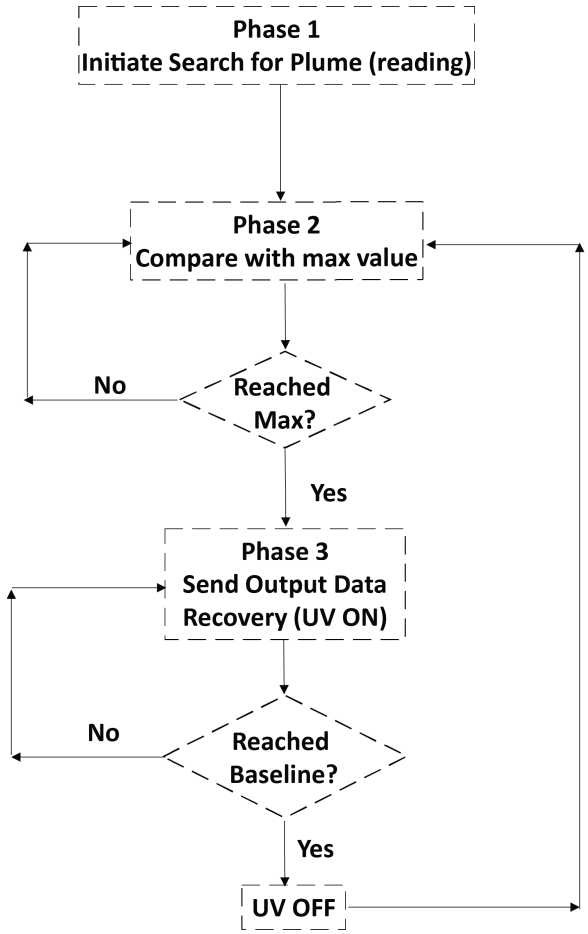

Fig. 12. Different phases in the UV-recovery-based plume mapping algorithm.

(defined from the result presented in Fig. 11), i.e., when the sensor's resistance crosses the maximum value, the next phase is triggered and the sensor sends output data. Simultaneously, the UV is turned ON (phase 3: send output data; UV ON). In the next phase the sensor response is compared with baseline value. UV will be off if the sensor reaches its baseline; otherwise, further recovery will be carried out. The UV-based recovery reduces the recovery time and consequently detection time of MONC functionalized MWCNT methane sensors by utilizing strong UV response of functionalizing MONCs.

VI. Sensor Response Time and Interferences

The current generation of the sensors showed response time of 15 min (Fig. 11) It has been reported that the long response time of CNT chemoresistive sensors might be a result of the slow diffusion and weaker absorption of the gas molecules onto the sensor surface [23]–[26].

Reduced dimension of the functionalizing ZnO nanocrystals might help improve the diffusion and absorption of the gas molecules by creating a larger number of active sites, i.e., more metal oxide sites. Reducing the dimension of the ZnO nanocrystals can be achieved in two ways: (1) reducing the number of ALD cycles when functionalizing the MWCNTs with ZnO, which reduces the thickness of the ZnO NCs and improves their discreteness on the MWCNT surface and (2) in related work, we observed that the mean size of the functionalizing ZnO NCs on MWCNTs becomes smaller as the ALD temperature increases [16]. The crystalline quality of the functionalizing ZnO NPs also improves with a higher temperature ALD. In the future, we plan to fabricate sensors with smaller sized NPs by increasing the ALD temperature. We expect a shorter response time from this next generation of sensors.

It was reported that ZnO functionalized CNT based chemoresistor sensors are sensitive to CO [27], NO_2 [28], H_2O, O_2 and H_2 [29]. To study the response of the sensor to relative humidity (RH), the resistance of the ZnO-MWCNT sensors at different RH was measured at room temperature by controlled flow of moist air inside an enclosed plastic chamber. The resistance of the sensor increased monotonically as the RH was increased from 10% to 91%. The resistance of the sensor returned to its initial value as the RH was reduced back to 10%. The highest recorded relative resistance change ($\Delta R/R = (R_{water} - R_{air})/R_{air}$) or the ZnO-MWCNT sensor was about 4% at 91% RH. Several preliminary tests with CO_2 were also performed. The ZnO-MWCNT sensor showed about 1.5% relative resistance at room temperature while exposed with 650 ppm of CO_2. However further experiments are required to verify sensitivity. Future plans include exposing the sensor to relevant levels of NO_2, H_2, and O_2 as well as additional testing with CO_2.

To address interference from other hydrocarbons present in natural gas, primarily ethane, we anticipate to use a combined signal from multiple sensors functionalized with different catalysts, akin to the electronic nose concept [30].

VII. Conclusion

We have fabricated a metal oxide nanocrystals (MONC) functionalized MWCNT-based CH_4 chemoresistor sensor capable of sensing below 10 ppm of CH_4 in dry air at room temperature. We presented a Gaussian plume model (GPM) based algorithm for a distributed methane sensor system (DMSS) which can use our chemoresistor sensor to localize leaks in natural gas infrastructure, such as production wells and pads. We present a localization algorithm, which can be used with the distributed sensors to pinpoint CH_4 leaks, allowing the DMSS to be used for continuous low-cost monitoring of CH_4 emission. We were able to reduce the recovery and consequently detection time of

functionalized MWCNT-based CH_4 sensors by utilizing strong UV response of functionalizing MONCs. Finally a UV-recovery-based plume detection algorithm is presented which offers acceleration in overall plume mapping process. Together with energy harvesting and ultra-low power wireless solutions this system can be used for ubiquitous monitoring of natural gas infrastructures such as production pads, valve stations and transmission pipelines.

ACKNOWLEDGMENT

The U.S. Environmental Protection Agency, through its Office of Research and Development, collaborated in the research described here. It has been subjected to Agency review and approved for publication.

REFERENCES

[1] *Climate Change 2007: Working Group I: The Physical Science Basis*, accessed on Jun. 29, 2016. [Online]. Available: http://www.ipcc.ch/publications_and_data/ar4/wg1/en/ch2s2-10-2.html

[2] *Overview of Greenhouse Gases*, accessed on Jun. 29, 2016. [Online]. Available: http://epa.gov/climatechange/ghgemissions/gases/ch4.html

[3] C. W. Rella, J. Hoffnagle, Y. He, and S. Tajima, "Local- and regional-scale measurements of CH_4, $\delta^{13}CH_4$, and C_2H_6 in the Uintah basin using a mobile stable isotope analyzer," *Atmos. Meas. Techn.*, vol. 8, no. 10, pp. 4539–4559, 2015.

[4] M. Humayun *et al.*, "Functionalized multi-walled carbon nanotube based sensors for distributed methane leak detection," in *Proc. IEEE SENSORS*, Nov. 2015, pp. 1–4.

[5] C. Massie, G. Stewart, G. McGregor, and J. R. Gilchrist, "Design of a portable optical sensor for methane gas detection," *Sens. Actuators B, Chem.*, vol. 113, no. 2, pp. 830–836, Feb. 2006.

[6] C. H. Wang *et al.*, "Detection of nitrogen dioxide using a room temperature operation mid-infrared InSb light emitting diode," *Electron. Lett.*, vol. 34, no. 3, pp. 300–301, Feb. 1998.

[7] *Measurement of the Carbon Isotopic Ratio of Atmospheric Methane*, accessed on Jun. 29, 2016. [Online]. Available: http://cfpub.epa.gov/ncer_abstracts/index.cfm/fuseaction/display.abstractDetail/abstract/6351/report/0

[8] D. Barreca *et al.*, "1D ZnO nano-assemblies by plasma-CVD as chemical sensors for flammable and toxic gases," *Sens. Actuators B, Chem.*, vol. 149, no. 1, pp. 1–7, Aug. 2010.

[9] P. Fau *et al.*, "Nanosized tin oxide sensitive layer on a silicon platform for domestic gas applications," *Sens. Actuators B, Chem.*, vol. 78, nos. 1–3, pp. 83–88, Aug. 2001.

[10] T. Waitz, T. Wagner, T. Sauerwald, C.-D. Kohl, and M. Tiemann, "Ordered mesoporous In_2O_3: Synthesis by structure replication and application as a methane gas sensor," *Adv. Funct. Mater.*, vol. 19, no. 4, pp. 653–661, Feb. 2009.

[11] T. Zhang, S. Mubeen, N. V. Myung, and M. A. Deshusses, "Recent progress in carbon nanotube-based gas sensors," *Nanotechnology*, vol. 19, no. 33, p. 332001, 2008.

[12] M. S. Dresselhaus, G. Dresselhaus, and R. Saito, "Physics of carbon nanotubes," *Carbon*, vol. 33, no. 7, pp. 883–891, 1995.

[13] Y. Lu *et al.*, "Room temperature methane detection using palladium loaded single-walled carbon nanotube sensors," *Chem. Phys. Lett.*, vol. 391, nos. 4–6, pp. 344–348, Jun. 2004.

[14] G. Lu, L. E. Ocola, and J. Chen, "Room-temperature gas sensing based on electron transfer between discrete tin oxide nanocrystals and multiwalled carbon nanotubes," *Adv. Mater.*, vol. 21, no. 24, pp. 2487–2491, Jun. 2009.

[15] J. Kong, M. G. Chapline, and H. Dai, "Functionalized carbon nanotubes for molecular hydrogen sensors," *Adv. Mater.*, vol. 13, no. 18, pp. 1384–1386, Sep. 2001.

[16] M. T. Humayun *et al.*, "ZnO functionalization of multiwalled carbon nanotubes for methane sensing at single parts per million concentration levels," *J. Vac. Sci. Technol. B*, vol. 33, no. 6, p. 06FF01, 2015.

[17] M. T. Humayun, R. Divan, Y. Liu, L. Gundel, P. A. Solomon, and I. Paprotny, "Novel chemoresistive CH_4 sensor with 10 ppm sensitivity based on multiwalled carbon nanotubes functionalized with SnO_2 nanocrystals," *J. Vac. Sci. Technol. A*, vol. 34, no. 1, p. 01A131, 2016.

[18] *National Wind Technology Center*, accessed on Jun. 29, 2016. [Online]. Available: http://www.nrel.gov/midc/nwtc_m2/

[19] J. H. Seinfeld and S. N. Pandis, *Atmospheric Chemistry and Physics: From Air Pollution to Climate Change*, 2nd ed. New York, NY, USA: Wiley, 2006.

[20] D. S. Kim *et al.*, "Synthesis and optical properties of ZnO and carbon nanotube based coaxial heterostructures," *Appl. Phys. Lett.*, vol. 93, no. 10, p. 103108, 2008.

[21] Y. Zhu *et al.*, "Multiwalled carbon nanotubes beaded with ZnO nanoparticles for ultrafast nonlinear optical switching," *Adv. Mater.*, vol. 18, no. 5, pp. 587–592, Mar. 2006.

[22] V. Dobrokhotov *et al.*, "Thermal and optical activation mechanisms of nanospring-based chemiresistors," *Sensors*, vol. 12, no. 5, pp. 5608–5622, 2012.

[23] A. Biaggi-Labiosa *et al.*, "A novel methane sensor based on porous SnO_2 nanorods: Room temperature to high temperature detection," *Nanotechnology*, vol. 23, no. 45, p. 455501, Nov. 2012.

[24] S. T. Shishiyanu, T. S. Shishiyanu, and O. I. Lupan, "Sensing characteristics of tin-doped ZnO thin films as NO_2 gas sensor," *Sens. Actuators B, Chem.*, vol. 107, no. 1, pp. 379–386, May 2005.

[25] N. D. Hoa *et al.*, "On-chip fabrication of SnO_2-nanowire gas sensor: The effect of growth time on sensor performance," *Sens. Actuators B, Chem.*, vol. 146, no. 1, pp. 361–367, Apr. 2010.

[26] S. Roy and S. Basu, "Improved zinc oxide film for gas sensor applications," *Bull. Mater. Sci.*, vol. 25, no. 6, pp. 513–515, Nov. 2002.

[27] J. Khanderi, R. C. Hoffmann, A. Gurlo, and J. J. Schneider, "Synthesis and sensoric response of ZnO decorated carbon nanotubes," *J. Mater. Chem.*, vol. 19, no. 28, pp. 5039–5046, Jun. 2009.

[28] B. A. Albiss, W. A. Sakhaneh, I. Jumah, and I. M. Obaidat, "NO_2 gas sensing properties of ZnO/single-wall carbon nanotube composites," *IEEE Sensors J.*, vol. 10, no. 12, pp. 1807–1812, Dec. 2010.

[29] O. Lupan, G. Chai, and L. Chow, "Novel hydrogen gas sensor based on single ZnO nanorod," *Microelectron. Eng.*, vol. 85, no. 11, pp. 2220–2225, Nov. 2008.

[30] A. Star, V. Joshi, S. Skarupo, D. Thomas, and J.-C. P. Gabriel, "Gas sensor array based on metal-decorated carbon nanotubes," *J. Phys. Chem. B*, vol. 110, no. 42, pp. 21014–21020, 2006.

Md Tanim Humayun received the B.Sc. degree in electrical and electronic engineering from the Bangladesh University of Engineering and Technology in 2008. He is currently pursuing the Ph.D. degree with the Department of Electrical and Computer Engineering, University of Illinois at Chicago, USA. He is a certified cleanroom user with the Center for Nanoscale Materials, Argonne National Laboratory, Lemont, IL. He is currently an Affiliate Researcher with the Lawrence Berkeley National Laboratory, Berkeley, CA. His research interests involve growth and synthesis of 1-D and 2-D materials, and characterization of their morphology, chemical composition, and crystal quality using various microscopy and spectroscopy techniques. His expertise also includes nanoscale device design, fabrication, and characterization with an emphasis on carbon nanotube gas sensors.

Ralu Divan received the M.Sc. and Ph.D. degrees in chemistry from the University of Bucharest, in 1977 and 1999, respectively. She has been with the Argonne National Laboratory since 1999. She is a Chemist with the Center for Nanoscale Materials, Argonne National Laboratory. She has micro and nanofabrication expertise with over 30 years of experience in materials, processes, and device integration. She developed and ran international projects in LIGA technology, silicon, germanium, metal, and glass micromachining for micromechanics and micro-optics. She has authored over 160 papers in journals and conference proceedings, two patents, and is a recipient of an RD 100 Award. Her expertise is in the area of development of high resolution, high aspect ratio lithographic processes by development of etching and growth processes for advanced micro and nanodevices, characterizing chemical and lithographic properties of materials, synthesis of nanoparticles and their use in micronanodevices, characterizing interfacial and compatibility properties of materials used in MEMS and NEMS, and development of membrane-based devices.

Liliana Stan received the B.S. degree in physics from the University of Bucharest, Romania, and the M.S. degree in electrical engineering from the University of New Mexico. She was a Scientist with the Los Alamos National Laboratory, where she played a key role in the design, characterization, and optimization of multilayered thin films for high-temperature superconductors and for electronic devices. She joined the Center for Nanoscale Materials, Argonne National Laboratory, in 2010, as a Senior Engineering Specialist.

Her expertise includes designing, synthesis, and characterization of multilayered structures of metal, dielectric, complex-oxide films, and multifunctional nanocomposites using physical vapor deposition techniques and atomic layer deposition. She has authored over 50 publications and holds six patents. Her research interests are centered on the development of functional structures incorporating functional complex oxides for electronic devices, metamaterials for nanophotonic and plasmonic applications, and materials for energy storage applications.

Daniel Rosenmann received the B.S. degree in physics from the Universidad Nacional Mayor de San Marcos, Lima, Peru, in 1986, and the M.S. degree in physics from Northern Illinois University in 2007. He has been an Argonne National Laboratory Staff Member since 1996 and currently a Principal Engineer Specialist with the Nanoscience and Technology Division at Argonne. His research interests include thin films and materials for sensors and device fabrication with an emphasis on probe development for SX-STM, an emerging scanning probe technique for imaging of nanoscale materials, which combines the subnanometer spatial resolution of SPM with the chemical, electronic, and magnetic sensitivity of synchrotron radiation.

David Gosztola received the B.S. degree in chemistry from Indiana University and the Ph.D. degree in analytical chemistry from Purdue University. He is currently a Staff Scientist with the Argonne National Laboratory's Center for Nanoscale Materials (a U.S. Department of Energy funded user facility) working in the Nanophotonics and Biofunctional Structures Group. His research interests include the development of laser-based instrumentation for investigating the interaction of light with nanoscale materials, ultrafast hotochemistry, interfacial dynamics, electrochemistry, and ultrafast laser-based instrumentation design.

Lara Gundel received the Ph.D. degree in physical chemistry from the University of California at Berkeley in 1975. She is currently a Staff Scientist with the Environmental Technologies Area of Lawrence Berkeley National Laboratory (LBNL), and a Co-Leader of the Air Microfluidics Group, a collaboration of the University of Illinois at Chicago, the University of California Berkeley, LBNL, and Argonne National Laboratory. At LBNL, she leads interdisciplinary projects that develop new approaches for characterizing air pollutants for public health-related applications. In 2000, she received an R&D 100 Award for a related invention. After establishing proof-of-concept for miniaturization of real-time sensors for mass concentration of fine particulate matter, her team began collaborating with the Berkeley Sensor & Actuator Center in 2005 to develop microfabricated sensors for airborne particles.

Paul A. Solomon received the B.S. (Hons.) degree in chemistry from the University of Maryland, College Park, MD, and the Ph.D. degree in analytical chemistry from the University of Arizona, Tucson, AZ. He was a Postdoctoral Research Assistant with the California Institute of Technology, Pasadena, CA. He is currently a Senior Research Scientist with the U.S. Environmental Protection Agency, National Exposure Research Laboratory, Exposure Methods and Measurements Division, and Sensing and Spatial Analysis Branch, Las Vegas, NV. His research interest primarily focus on developing, improving, and applying analytical and air sampling methods to characterize and quantify major, minor, and trace elements and species in ambient air. Most recently, his interests have focused on developing air pollution sensors for PM mass, black carbon, and methane and their application employing mobile, stationary, and personal monitoring platforms to obtain hyperlocal air quality information that can be used to inform individuals and communities empowering them to reduce their exposures to air pollution.

Igor Paprotny is an Assistant Professor with the Department of Electrical and Computer Engineering, University of Illinois, Chicago (UIC). He also holds an Affiliate Scientist position at Lawrence Berkeley National Laboratory, and is the lead of the Air-Microfluidics Group (AMFG). Prior to his appointment at UIC, he was a post-doc and later a Research Scientist at UC Berkeley. Over the past six years, he has successfully led work on a number of energy and sensor related projects funded by the California Energy Commission. He is currently advising or co-advising 11 graduate students and one postdoc working on a variety of problems related to robotics, energy systems sensing, and air-microfluidics at UIC and at UC Berkeley. He has published five book chapters and over 50 papers in journals and conferences, as well as is the coauthor on four patents. His expertise is on design, modeling, and fabrication of mechatronic devices based on microelectromechanical systems.